

# Emergent Spinon Dispersion and Symmetry Breaking in Two-channel Kondo Lattices

Yang Ge and Yashar Komijani\*

Department of Physics, University of Cincinnati, Cincinnati, Ohio, 45221, USA

(Dated: January 19, 2022)

Two-channel Kondo lattice serves as a model for a growing family of heavy-fermion compounds. We employ dynamical large- $N$  technique and go beyond the independent bath approximation to study this model both numerically and analytically using renormalization group ideas. We show that Kondo effect induces dynamic magnetic correlations that lead to an emergent spinon dispersion. Furthermore, we develop a quantitative framework that interpolates between infinite dimension where the channel-symmetry broken results of mean-field theory are confirmed, and one-dimension where the channel symmetry is restored and a critical fractionalized mode is found.

The screening of a magnetic impurity by the conduction electrons in a metal is governed by the Kondo effect. The multi-channel version is when several channels compete to a single impurity, as a result of which the spin is frustrated and a new quantum critical groundstate forms with a fractional residual impurity entropy. In the two-channel case, this entropy  $\frac{1}{2} \log 2$  corresponds to a Majorana fermion. If the channel symmetry is broken, the weaker channels decouple and the stronger-coupled channels *win* to screen the impurity at low temperature [1–4].

While the case of a single impurity is well understood, much less is known about Kondo lattices where a lattice of spins is screened by conduction electrons [5, 6], especially if multiple conduction channels are involved [7]. The most established fact is the prediction of a large Fermi surface (FS) in the Kondo-dominated regime of the single-channel Kondo lattice [8]. In the multi-channel case, the continuous channel symmetry naturally leads to new patterns of entanglement which are potentially responsible for the non-Fermi liquid physics [9, 10], but also symmetry breaking and possibly fractionalized order parameter [11]. This partly arises from the fact that the residual entropy seen in the impurity has to eventually disappear at zero temperature in the case of the lattice.

Beside fundamental interest, a pressing reason for studying this physics is that the multi-channel Kondo lattice (MCKL), and in particular 2CKL, seem to be an appropriate model for several heavy-fermion compounds, e.g. the family of  $\text{PrTr}_2\text{Z}_{20}$  ( $\text{Tr}=\text{Ir,Rh}$ ) [12, 13] as well as the recent proposal that topological defects in MCKLs [14] might realize non-abelian Kondo anyons [15, 16].

The MCKL model is described by the Hamiltonian

$$H = H_c + J_K \sum_j \vec{S}_j \cdot c_{ja}^\dagger \vec{\sigma} c_{ja} \quad (1)$$

where  $H_c = -t_c \sum_{\langle ij \rangle} (c_{i\alpha a}^\dagger c_{j\alpha a} + h.c.)$  is the Hamiltonian of the conduction electrons and Einstein summation over spin  $\alpha, \beta = 1 \dots N$  and channel  $a, b = 1 \dots K$  indices is assumed. This model has  $\text{SU}(N)$  spin and  $\text{SU}(K)$  channel symmetries and we are interested to analyze the effect of a channel (ch.) symmetry breaking  $H \rightarrow H + \sum_j \Delta \vec{J}_j \cdot \vec{O}_j$ , where  $\vec{O}_j \equiv (\vec{S}_j \cdot c_{ja}^\dagger \vec{\sigma} c_{jb}) \vec{\tau}_{ba}$  and  $\vec{\tau}$ -s act as Pauli matrices in the channel space.

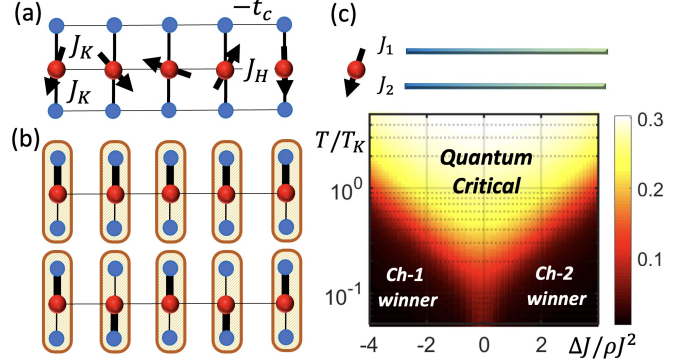


FIG. 1. (a) The 1D version of the two-channel Kondo lattice model studied here. (b) The strong coupling leads to a channel magnet; two different patterns of channel symmetry breaking, ch. FM (top) and ch. AFM (bottom). Bold lines represents spin-singlets. (c) The entropy  $S$  of two-channel Kondo impurity vs. ch. asymmetry and temperature. At the symmetric point,  $S$  reduces to a fraction of the high- $T$  value.

At first look, at least certain deformation [17] of the MCKL can be thought of as a channel magnet. In the  $J_K \rightarrow \infty$  limit [18], the spin is quenched due to formation of Kondo singlet with either (for  $K = 2$ ) of channels, leading to a doublet over which  $\vec{O}$  acts like  $\vec{\tau}$  [18]. Interaction among adjacent doublets leads to a “channel magnet”  $H_{\text{eff}} \propto \frac{t^2}{J_K} \sum_{\langle ij \rangle} \vec{O}_i \cdot \vec{O}_j$ . While channel Weiss-field favors a ch. anti-ferromagnetic (ch. AFM) super-exchange interaction, the mean-field theory predicts a variety of ch. ferromagnetic (ch. FM) and ch. AFM solutions [Fig. 1(b)] depending on the conduction filling.

On the other hand, some differences to a channel magnet are expected since the winning channel has a larger FS [11, 19] and the order parameter  $\vec{O}$  is strongly dissipated by coupling to fermionic degrees of freedom. Although a channel-symmetry broken groundstate is predicted by both dynamical mean-field theory (DMFT) [20, 21] and static mean-field theory [19, 22, 23], it has been questioned by recent quantum Monte Carlo results [24]. Furthermore, the effective theory of fluctuations in the large- $N$  limit [19] predicts a disordered phase below the lower critical dimension but the nature of this quan-

tum paramagnet is unclear. In 1D, Andrei and Orignac have used bosonization to show [25] that the groundstate is gapless and fractionalized (dispersing Majoranas for  $K = 2$ ), a prediction that has *not* been confirmed by the density matrix renormalization group calculations [26].

Resolving these issues requires a technique that is applicable to arbitrary dimensions and goes beyond static mean-field and DMFT by capturing both quantum and spatial fluctuations. Here we show that dynamical large-N approach, recently applied successfully to study Kondo lattices [16, 27–34], is precisely such a technique.

We assume the spins transform as a spin- $S$  representation of  $SU(N)$ . In the impurity case [35], the spin is fully screened for  $K = 2S$  whereas it is over/under-screened for  $K > 2S$  and  $K < 2S$ , respectively [36]. The focus of this paper is on the Kondo-dominated regime of the double-screened case  $K/2S = 2$  which is schematically shown in Fig. 1(a). We use Schwinger bosons  $S_{j\alpha\beta} = b_{j\alpha}^\dagger b_{j\beta}$  to form a symmetric representation of spins with the size  $2S = b_{j\alpha}^\dagger b_{j\alpha}$ . We then rescale  $J_K \rightarrow J_K/N$  and treat the model (1) in the large- $N$  limit, by sending  $N, K, S \rightarrow \infty$ , but keeping  $s = S/N$  and  $\gamma = K/N = 4s$  constant. The constraint is imposed on average via a uniform Lagrange multiplier  $\mu_b$ .

In the present large- $N$  limit, the RKKY interaction is  $O(1/N)$  [inset of Fig. 2(a)] and we need to include an explicit Heisenberg interaction  $H \rightarrow H + J_H \sum_{\langle ij \rangle} \vec{S}_i \cdot \vec{S}_j$  between nearest neighbors  $\langle ij \rangle$  to couple the impurities. Nevertheless, we will show that an infinitesimal  $J_H$  is sufficient to produce significant magnetic correlations due to a novel variant of RKKY interaction. For simplicity we limit ourselves to ferromagnetic correlations  $J_H < 0$ .

For a  $\mathcal{V}$  site lattice, the Lagrangian becomes [28, 37]

$$\mathcal{L} = \sum_k \bar{c}_{ka\alpha} (\partial_\tau + \epsilon_k) c_{ka\alpha} + \sum_k \bar{b}_{k\alpha} (\partial_\tau + \epsilon_k) b_{k\alpha} - 2\mathcal{V}\lambda S + \sum_j \frac{\bar{\chi}_{ja}\chi_{ja}}{J_K} + \sum_j \frac{1}{\sqrt{N}} (\bar{\chi}_{ja} b_{j\alpha} \bar{c}_{ja\alpha} + h.c.). \quad (2)$$

Here,  $b$ -s are bosonic spinons and  $\chi$ -s are Grassmannian holons that mediate the local Kondo interaction. In momentum space, the electrons and bosons have dispersions  $\epsilon_k = -2t_c \cos k - \mu_c$  and  $\epsilon_k = -2t_b \cos k - \mu_b$ , respectively.  $t_b$  is the (assumed to be homogenous) nearest neighbor hopping of spinons due to large- $N$  decoupling of  $J_H$  term [18]. Here, we focus on a half-filled conduction band  $\mu_c = 0$ , but similar results are obtained at other commensurate fillings [18]. In the large- $N$  limit the dynamic is dominated by the non-crossing Feynman diagrams, resulting in boson and holon self-energies [ $\vec{r} \equiv (j, \tau)$ ]

$$\Sigma_b(\vec{r}) = -\gamma G_c(\vec{r}) G_\chi(\vec{r}), \quad \Sigma_\chi(\vec{r}) = G_c(-\vec{r}) G_b(\vec{r}), \quad (3)$$

whereas  $\Sigma_c$  is  $O(1/N)$  and thus the electrons propagator  $G_c^{-1}(k, z) = z - \epsilon_k$  remains bare, with  $z$  complex frequency. Eqs. (3) together with the Dyson equations

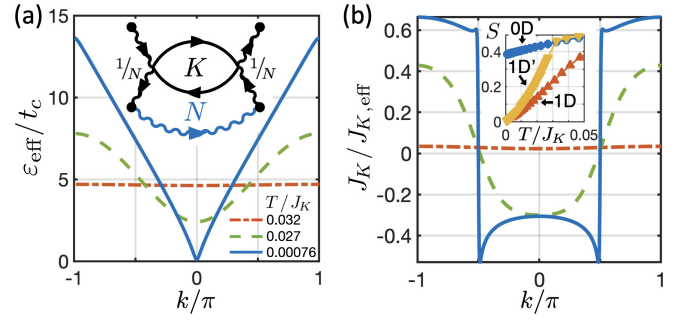


FIG. 2. 1D 2CKL model. The temperature evolution of (a) the effective energy  $\epsilon_{\text{eff}}$  for spinons and (b) the inverse effective Kondo coupling  $J_{K,\text{eff}}^{-1}$  for holons. At high- $T$ ,  $J_{K,\text{eff}} = J_K$  with no  $k$  dependence. Initially, Kondo effect develops locally and  $J_{K,\text{eff}}^{-1} \rightarrow 0$ . Then dispersion emerges in both  $G_\chi$  and  $G_b$ , with  $J_{K,\text{eff}}^{-1}$  vanishing only at  $k \approx \pm k_F$  and  $\epsilon_{\text{eff}}$  only at  $k \approx 0$ . Inset of (a): Despite an  $O(1/N)$  RKKY interaction (black), an initial spinon dispersion (blue) can lead to an  $O(1)$  amplification in the present over-screened case. Inset of (b): Entropy  $S$  vs.  $T$  for 0D, 1D ( $t_b = 0.2t_c$ ) and 1D' ( $t_b = 0.0002t_c$ ).

$G_b^{-1}(k, z) = z - \epsilon_k - \Sigma_b(k, z)$  and  $G_{\chi,a}^{-1}(k, z) = -J_{K,a}^{-1} - \Sigma_\chi(k, z)$  form a set of coupled integral equations that are solved iteratively and self-consistently, while  $\mu_b$  is adjusted to satisfy the constraint. Thermodynamic variables are then computed from Green's functions [27, 28].

First, we study the case in which  $J_H$  is absent, or  $\epsilon_k = -\mu_b$ . In this limit, the self-energies remain local  $\Sigma_{b,\chi}(n, \tau) \rightarrow \delta_{n0} \Sigma_{b,\chi}(\tau)$  and the problem reduces to the impurity problem [37]. It has never been studied whether the large- $N$  over-screened impurities are susceptible to symmetry breaking [2]. To do so, we assume that half of  $K$  channels are coupled to the impurity with  $J_K + \Delta J_K$  and the other half with  $J_K - \Delta J_K$ . This corresponds to a uniform symmetry breaking deformation  $\Delta\mathcal{L} = (\Delta J/J_K^2) \sum_j [\bar{\chi}_{j1}\chi_{j1} - \bar{\chi}_{j2}\chi_{j2}]$  of the Lagrangian. Fig. 1(c) shows the entropy of the 2CK impurity model as a function of channel asymmetry, verifying that the impurity is indeed critical w.r.t. channel symmetry breaking.

Next, we focus on finite  $t_b$  case for two settings of 1D and  $\infty$ D, which correspond to a Bethe lattice with coordination numbers  $z = 2$  and  $z = \infty$ . In 1D,  $G(k, z)$  and  $\Sigma(k, z)$  depend on  $k$  and  $z$ , but in  $\infty$ D, self-energies have no spatial dependence and the Green's functions of spinons/electrons obey  $G_{b,c}^{-1} = z - \mu_{b,c} - \Sigma_{b,c}(z) - t_{b,c}^2 G_{b,c}$ .

Importantly, the criticality of over-screened impurity solution ensures that an infinitesimal spinon hopping seed  $t_b \sim 0$  can get an  $O(1)$  amplification [inset of Fig. 2(a)] and a dispersion for spinons and holons is *dynamically* generated. Restricting ourselves to translationally invariant solutions with periodicity of a lattice constant  $a$ , a succinct measure of this effect is the zero frequency spinon/holon effective dispersion  $J_{K,\text{eff}}^{-1}(k) \equiv -\text{Re}[G_\chi^{-1}(k, \omega = 0)]$  and  $\epsilon_{\text{eff}}(k) \equiv -\text{Re}[G_b^{-1}(k, \omega = 0)]$ , shown in Fig. 2(a,b) for various temperatures. This emer-

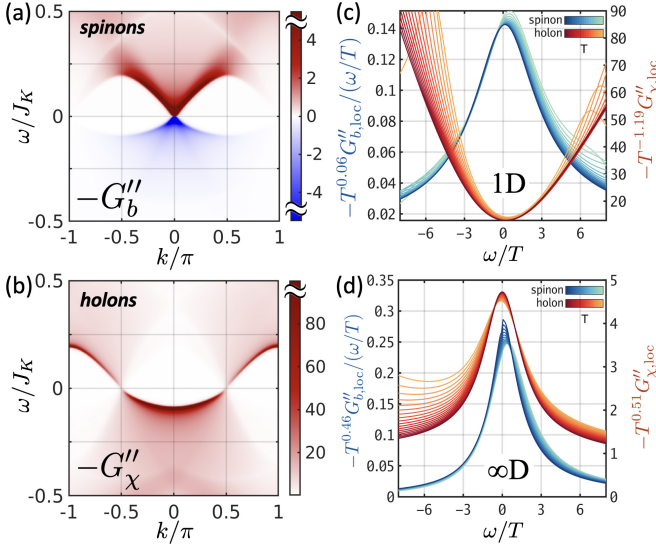


FIG. 3. The spectral function of (a) spinons and (b) holons in a 1D two-channel Kondo lattice at  $T/J_K = 0.0072$ , showing emergent linearly-dispersing spinons at  $k = 0$  (bare dispersion is quadratic) and holons with Fermi point at  $\pm k_F$ . Scaling collapse of spinon and holon Green's functions in the 2CK critical regime in (c) 1D lattice ( $z = 2$ )  $0.0072 \leq T/J_K \leq 0.03$  and (d)  $\infty$ D Bethe lattice ( $z = \infty$ )  $0.006 \leq T/J_K \leq 0.03$ . For both cases,  $J_K/t = 6$ ,  $t_b/t = 0.2$ , and  $s = 0.15$ .

gent spinon dispersion is independent of the choice of the seed and agree qualitatively with the finite  $t_b$  results [18]. The consumption of the residual entropy in the lattice by the emerging dispersion is visible in the inset of Fig. 2(b).

Fig. 3(a,b) shows the finite frequency spectral function of spinons and holons, respectively. Both are dominated by a sharp mode. The spinons are gapless and linearly dispersing (emergent Lorentz invariance) and the holons form a FS. The temperature collapse of Fig. 3(c) confirms that the spectra are critical with the local spectra obeying a  $T^{1-2\Delta_b, \chi} G''_{b, \chi}(x=0, \omega) = f_{b, \chi}(\omega/T)$  behavior. Fig. 3(d) shows similar collapse for the case of infinite-Coordination Bethe lattice ( $\infty$ D). A marked difference between the two cases is that  $\Delta_\chi > 1/2$  for 1D, which leads to  $-G''_\chi$  minima at  $\omega \sim 0$ , whereas  $\Delta_\chi < 1/2$  in  $\infty$ D, manifested as a peak at  $\omega \sim 0$ .

What is the effect of channel symmetry breaking on the volume of FS? According to Luttinger's theorem, the FS volume is related to electron phase shift  $v_{\chi, a}^{\text{FS}} = \mathcal{V}^{-1} \sum_k \delta_a(k)$ . From  $K = 4S$  case of the Ward identity [38], the electron phase shift is related to that of holons  $N\delta_{c, a}(k) = \delta_{\chi, a}(k)$ , which itself is defined as

$$\delta_{\chi, a}(k) = -\text{Im}\{\log[-G_{\chi, a}^{-1}(k, 0 + i\eta)]\}. \quad (4)$$

In 1D, holons are occupied for  $|k| < \pi/2$ . So, we find that  $v_{\chi, a}^{\text{FS}} = 2\pi S/K = \pi/2$  and the total change in electron FS is  $N\Delta v_{c, a}^{\text{FS}} = \pi/2$ , corresponding to a large FS in the critical phase. We use Eq. (4) to study the effect of a uniform symmetry breaking field  $\Delta\mathcal{L}$ . Fig. 4(a) shows how

FSs of slightly favored and disfavored channels evolve as a function of  $T$  in the two cases. In 1D, the FS asymmetry disappears, restoring a ch. symmetric criticality at low  $T$ . On the other hand in  $\infty$ D the asymmetry grows and one channel totally decouples from the spins, with gapped spinons and holons for both channels. The exponents are related to  $\Delta_\chi$ ; varying  $\Delta J$  in Eq. (4) we find  $\partial v_{\chi, a}^{\text{FS}}/\partial\Delta J = -G''_\chi(x=0, 0 + i\eta)$ . Using the scaling collapse,  $\partial v_{\chi, a}^{\text{FS}}/\partial\Delta J \sim T^{2\Delta_\chi - 1}$ , agreeing with Fig. 4(a) and confirming  $\Delta_\chi = 1/2$  as the marginal dimension.

Fig. 4(a) suggests that the symmetry breaking  $\Delta\mathcal{L}$  is relevant in  $\infty$ D, in the renormalization group (RG) sense, but is irrelevant in 1D. To establish this from the microscopic Hamiltonian, one has to access the infrared (IR) fixed point. From the numerics we see that the system flows to a critical IR fixed point, in which spinons and holons are critical in addition to electrons. For an impurity  $G_b \sim |\tau|^{-2\Delta_b}$  and  $G_\chi(\tau) \sim |\tau|^{-2\Delta_\chi}$  are reasonable ansatzes at  $T = 0$ . The exponents are known [18, 37]:

$$0, \infty\text{D}: \quad \Delta_\chi = \frac{\gamma}{2(1+\gamma)}, \quad \Delta_b = \frac{1}{2(1+\gamma)}, \quad (5)$$

and coincide with those of the  $\infty$ D in the small  $t_b$  regime we are interested here [18]. In presence of a dimensionless  $\lambda_0 = \Delta J/\rho J_K^2$ , the RG analysis  $d\lambda/dl = (1 - 2\Delta_\chi)\lambda$  predicts a dynamical scale  $w \sim T_K \lambda_0^{1+\gamma}$  [c.f. Fig. 1(c)].

The 1D case is more subtle; as  $T \rightarrow 0$ , we see from Fig. 2 that  $J_{\text{eff}}^{-1}(\pm k_F) \rightarrow 0$  and  $\varepsilon_{\text{eff}}(0) \rightarrow 0$  at the IR fixed point [39]. This means that the Kondo coupling flows to strong coupling for  $|k| < k_F$  and to weak coupling at  $|k| > k_F$  and it is critical at  $k = \pm k_F$  and the spinons are gapless as  $k \rightarrow 0$ . At these points, the Dyson equation has the form  $G_b \Delta \Sigma_b|_{k \approx 0} = G_\chi \Delta \Sigma_\chi|_{k \approx \pm k_F} = -1$ .

We can obtain a low-energy description by expanding fields near zero energy, e.g.  $\psi(x) \sim e^{ik_F x} \psi_R + e^{-ik_F x} \psi_L$  for electrons and holons. In 1+1 dimensions, the conformal invariance of the fixed point dictates the following form for the  $T = 0$  Green's functions  $G(x, \tau) = G(z, \bar{z})$ :

$$G_b = -\bar{\rho} \left(\frac{a^2}{zz}\right)^{\Delta_b}, \quad G_{\chi R/L} = \frac{-1}{2\pi} \left(\frac{a}{z}\right)^{\Delta_\chi \pm \frac{1}{2}} \left(\frac{a}{\bar{z}}\right)^{\Delta_\chi \mp \frac{1}{2}} \quad (6)$$

where  $z = v\tau + ix$  and  $\bar{\rho} = 2s/a$ . The  $G_{cR/L}$  is obtained from  $G_{\chi R/L}$  by  $\Delta_\chi \rightarrow 1/2$ . These Green's functions can be conformally mapped to finite- $T$  via  $z \rightarrow (\beta/\pi) \sin(\pi z/\beta)$  replacement. Furthermore, in terms of  $q = k + i\omega/v$ , they have the Fourier transforms:

$$G_b = -2\pi a^2 \bar{\rho} v_b^{-1} (a^2 \bar{q} q)^{\Delta_b - 1} \zeta_0(\Delta_b) \quad (7)$$

$$G_{\chi R/L} = \mp a^2 v_\chi^{-1} (a \bar{q})^{\Delta_\chi - 1 \mp 1/2} (a q)^{\Delta_\chi - 1 \pm 1/2} \zeta_1(\Delta_\chi)$$

where  $\zeta_n(\Delta) \equiv 2^{1-2\Delta} \Gamma(1 - \Delta + n/2)/\Gamma(n/2 + \Delta)$ . From matching the powers of frequency in Eqs. (3,6,7), we conclude that  $\Delta_b + \Delta_\chi = 3/2$  in order to satisfy the self-consistency. Moreover, from the matching of the amplitude of the Green's functions we find [18]

$$1\text{D}: \quad \Delta_\chi = \frac{1 + 6\gamma}{2(1 + 2\gamma)}, \quad \Delta_b = \frac{2}{2(1 + 2\gamma)}. \quad (8)$$



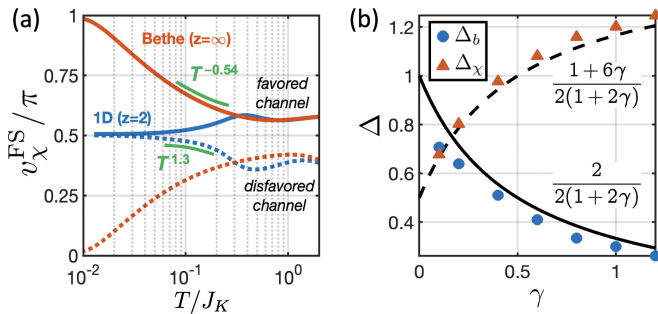


FIG. 4. (a) The evolution of FS in presence of small channel symmetry breaking in 1D and  $\infty$ D with temperature. (b) The scaling exponents  $\Delta_{b/\chi}$  in 1D from the numerics. The lines show the analytical values given by Eqs. (8).

Note that  $\Delta_\chi > 1/2$ , ensuring that channel symmetry breaking perturbations are irrelevant in 1D. These are in excellent agreement with the exponents extracted from  $\omega/T$  scaling [Fig. 4(b)] and we have established a semi-analytical framework to interpolate between 1D and  $\infty$ D.

The emergent dispersion in Fig. 2, the scaling dimensions in Eq. (8) and their relation to symmetry breaking in Fig. 4 are the central results of this paper. In the following we discuss some implications of these results.

The fractionalization  $S_{\alpha\beta} \sim b_\alpha^\dagger b_\beta$  or  $b_\alpha^\dagger c_{a\alpha} \sim \chi_a$  contraction are related to order parameter fractionalization [11, 40]. In the long time/distance limit, correlation functions of  $b_\alpha^\dagger c_{a\alpha}$  and that of  $\chi_a$  are given by  $\Sigma_\chi$  and  $G_\chi$ , respectively and thus, have exponents that add up to zero. On the other hand, correlators of gauge-invariant operators  $\mathcal{X}_{ab} \equiv \bar{\chi}_a \chi_b$  and  $\mathcal{O}_{ab} \equiv b_\alpha^\dagger b_\beta c_{b\beta}^\dagger c_{a\alpha}$  are exactly equal since both can be constructed by taking derivatives of free energy w.r.t.  $\Delta J^{ab}$  before/after Hubbard-Stratonovich transformation. A diagrammatic proof of this equivalence is provided in [18]. Scaling analysis gives  $\chi_{\text{ch}}(x=0) \sim T^{4\Delta_\chi-1}$  and  $\chi_{\text{ch}}^{\text{1D}}(q=0) \sim T^{4\Delta_\chi-2}$  up to a constant shift coming from the regular part of free energy.

Another non-trivial feature of 2CK impurity fixed point is its magnetic instability [2] whose large- $N$  incarnation is  $\Delta_b < 1/2$  for the impurity (or  $\infty$ D) in Eq. (5). From Eq. (8), we see that this also holds for 1D 2CKL for  $\gamma > 1/2$ . This is reflected in the divergence of the uniform  $\chi_m(q=0)$  static magnetic susceptibilities as a function of  $T$ . Using scaling analysis  $\chi_m^{\text{1D}}(q=0) \sim T^{4\Delta_b-2}$  and  $\chi_m(x=0) \sim T^{4\Delta_b-1}$  up to a constant shift, in good agreement with numerics [18].

Lastly, the 1+1 correlators (6) can be obtained from a Luttinger liquid model for each of the  $c, b, \chi$  fields with fine-tuned Luttinger parameters that give the correct exponents. Such a spinon-holon theory of will have a Virasoro central charge  $c_0/N = 1 + \gamma$ . It is curious whether the central charge is reduced compared to  $c_0$  due to interaction. However, it follows from  $\Delta_b + \Delta_\chi = 3/2$  and the large- $N$  limit that  $H_{\text{int}}$  in Eq. (2) is exactly marginal at the IR fixed point to  $O(1/N)$ . We have used  $T \rightarrow 0$

heat-capacity and the excitation velocities  $v$  to compute the central charge according to  $C/T = (\pi k_B^2/6v)c$  as a function of  $\gamma$ . Our results, summarized in [18], agree with  $c_0/N$ . The discrepancy with the coset theory of [18, 25]  $c_{AO}/N = 1 - (1 + \gamma)^{-2}$  is likely rooted in inability of Schwinger bosons to capture gapless spin-liquids [41].

In summary, we have shown that dynamical large- $N$  approach can capture symmetry breaking in multi-channel Kondo impurities and lattices in presence of both emergent and induced ferromagnetic correlations within an RG framework with explicit examples on 0D, 1D and  $\infty$ D. The scaling analysis enables an analytical solution to the critical exponents and susceptibilities which are in good quantitative agreement with numerics, and is applicable to higher dimensional CFTs. A determination of upper/lower critical dimensions and effect of anti-ferromagnetic correlation is left to a future work [42].

*Acknowledgment* — The authors acknowledge fruitful discussions with P. Coleman and N. Andrei and appreciate the hospitality of Aspen Center for Physics.

- 
- [1] N. Andrei and C. Destri, Solution of the multichannel Kondo problem, *Phys. Rev. Lett.* **52**, 364 (1984).
  - [2] I. Affleck, A. W. W. Ludwig, H.-B. Pang, and D. L. Cox, Relevance of anisotropy in the multichannel Kondo effect: Comparison of conformal field theory and numerical renormalization-group results, *Phys. Rev. B* **45**, 7918 (1992).
  - [3] V. J. Emery and S. Kivelson, Mapping of the two-channel Kondo problem to a resonant-level model, *Phys. Rev. B* **46**, 10812 (1992).
  - [4] I. Affleck and A. W. W. Ludwig, Exact conformal-field-theory results on the multichannel Kondo effect: Single-fermion Green's function, self-energy, and resistivity, *Phys. Rev. B* **48**, 7297 (1993).
  - [5] A. C. Hewson, *The Kondo Problem to Heavy fermions*, Cambridge Studies in Magnetism (Cambridge University Press, 1993).
  - [6] P. Coleman, *Introduction to Many-Body Physics* (Cambridge University Press, 2015).
  - [7] D. L. Cox and M. Jarrell, The two-channel Kondo route to non-Fermi-liquid metals, *J. Phys. Condens. Matter* **8**, 9825 (1996).
  - [8] M. Oshikawa, Topological approach to Luttinger's theorem and the Fermi surface of a Kondo lattice, *Phys. Rev. Lett.* **84**, 3370 (2000).
  - [9] M. Jarrell, H. Pang, D. L. Cox, and K. H. Luk, Two-channel Kondo lattice: An incoherent metal, *Phys. Rev. Lett.* **77**, 1612 (1996).
  - [10] M. Jarrell, H. B. Pang, and D. L. Cox, Phase diagram of the two-channel Kondo lattice, *Phys. Rev. Lett.* **78**, 1996 (1997).
  - [11] Y. Komijani, A. Toth, P. Chandra, and P. Coleman, Order fractionalization, [arXiv:1811.11115](https://arxiv.org/abs/1811.11115) (2018).
  - [12] T. Onimaru and H. Kusunose, Exotic quadrupolar phenomena in non-Kramers doublet systems — the cases of  $\text{PrT}_2\text{Zn}_{20}$  ( $T = \text{Ir, Rh}$ ) and  $\text{PrT}_2\text{Al}_{20}$  ( $T = \text{V, Ti}$ ) —, *J. Phys. Soc. Jpn.* **85**, 082002 (2019).

- [13] A. S. Patri and Y. B. Kim, Critical theory of non-Fermi liquid fixed point in multipolar Kondo problem, *Phys. Rev. X* **10**, 041021 (2020).
- [14] M. Kornjaca, V. L. Quito, and F. Rebecca, Mobile Majorana zero-modes in two-channel Kondo insulators, [arXiv:2104.11173](https://arxiv.org/abs/2104.11173) (2021).
- [15] P. L. S. Lopes, I. Affleck, and E. Sela, Anyons in multichannel Kondo systems, *Phys. Rev. B* **101**, 085141 (2020).
- [16] Y. Komijani, Isolating Kondo anyons for topological quantum computation, *Phys. Rev. B* **101**, 235131 (2020).
- [17] A naïve strong coupling limit is not a spin-singlet, the Nozières doublet, but see the supplementary material for a deformation that changes this.
- [18] See supplementary materials.
- [19] A. Wugalter, Y. Komijani, and P. Coleman, Large- $N$  approach to the two-channel Kondo lattice, *Phys. Rev. B* **101**, 075133 (2020).
- [20] S. Hoshino, J. Otsuki, and Y. Kuramoto, Diagonal composite order in a two-channel Kondo lattice, *Phys. Rev. Lett.* **107**, 247202 (2011).
- [21] S. Hoshino and Y. Kuramoto, Collective excitations from composite orders in Kondo lattice with non-Kramers doublets, *J. Phys. Conf. Ser.* **592**, 012098 (2015).
- [22] J. S. Van Dyke, G. Zhang, and R. Flint, Field-induced ferromagnetic phase in cubic non-Kramers doublet systems, *Phys. Rev. B* **100**, 205122 (2019).
- [23] G. Zhang, J. S. Van Dyke, and R. Flint, Cubic hastatic order in the two-channel Kondo-Heisenberg model, *Phys. Rev. B* **98**, 235143 (2018).
- [24] K. Inui and Y. Motome, Channel-selective non-Fermi liquid behavior in the two-channel Kondo lattice model under a magnetic field, *Phys. Rev. B* **102**, 155126 (2020).
- [25] N. Andrei and E. Orignac, Low-energy dynamics of the one-dimensional multichannel Kondo-Heisenberg lattice, *Phys. Rev. B* **62**, R3596 (2000).
- [26] T. Schauerer, D. L. Cox, R. M. Noack, P. G. J. van Dongen, and C. D. Batista, Phase diagram of the two-channel Kondo lattice model in one dimension, *Phys. Rev. Lett.* **94**, 147201 (2005).
- [27] J. Rech, P. Coleman, G. Zarand, and O. Parcollet, Schwinger boson approach to the fully screened Kondo model, *Phys. Rev. Lett.* **96**, 016601 (2006).
- [28] Y. Komijani and P. Coleman, Model for a ferromagnetic quantum critical point in a 1D Kondo lattice, *Phys. Rev. Lett.* **120**, 157206 (2018).
- [29] Y. Komijani and P. Coleman, Emergent critical charge fluctuations at the Kondo breakdown of heavy fermions, *Phys. Rev. Lett.* **122**, 217001 (2019).
- [30] J. Wang, Y.-Y. Chang, C.-Y. Mou, S. Kirchner, and C.-H. Chung, Quantum phase transition in a two-dimensional Kondo-Heisenberg model: A dynamical Schwinger-boson large- $N$  approach, *Phys. Rev. B* **102**, 115133 (2020).
- [31] B. Shen, Y. Zhang, Y. Komijani, M. Nicklas, R. Borth, A. Wang, Y. Chen, Z. Nie, R. Li, X. Lu, *et al.*, Strange-metal behaviour in a pure ferromagnetic Kondo lattice, *Nature* **579**, 51 (2020).
- [32] J. Wang and Y.-f. Yang, Nonlocal Kondo effect and quantum critical phase in heavy-fermion metals, *Phys. Rev. B* **104**, 165120 (2021).
- [33] V. Drouin-Touchette, E. J. König, Y. Komijani, and P. Coleman, Emergent moments in a Hund's impurity, *Phys. Rev. B* **103**, 205147 (2021).
- [34] R. Han, D. Hu, J. Wang, and Y.-f. Yang, Schwinger boson approach for the dynamical mean-field theory of the kondo lattice, *Phys. Rev. B* **104**, 245132 (2021).
- [35] We use 0D to refer to the impurity problem, although a conduction band exists.
- [36] P. Zinn-Justin and N. Andrei, The generalized multichannel Kondo model: Thermodynamics and fusion equations, *Nucl. Phys. B* **528**, 648 (1998).
- [37] O. Parcollet and A. Georges, Transition from overscreening to underscreening in the multichannel Kondo model: Exact solution at large  $N$ , *Phys. Rev. Lett.* **79**, 4665 (1997).
- [38] P. Coleman, I. Paul, and J. Rech, Sum rules and ward identities in the Kondo lattice, *Phys. Rev. B* **72**, 094430 (2005).
- [39] This is not the case for the spinon's  $\pi$ -mode  $\epsilon_{\text{eff}}(\pm\pi/a) \neq 0$ , but this mode has negligible spectral weight.
- [40] A. M. Tsvelik and P. Coleman, Order fractionalization in a kitaev-Kondo model, [arXiv:2112.07781](https://arxiv.org/abs/2112.07781) (2021).
- [41] D. P. Arovas and A. Auerbach, Functional integral theories of low-dimensional quantum Heisenberg models, *Phys. Rev. B* **38**, 316 (1988).
- [42] Y. Ge and Y. Komijani, in preparation.

## Supplementary materials

This supplementary material contains additional proofs, details and supporting materials for the statements made in the paper.

### 1. Strong coupling and channel magnet

We can use  $\text{SU}_{\text{sp}}(2) \otimes \text{SU}_{\text{ch}}(2) \otimes \text{U}(1)$  symmetries to label various local states of the two-channel Kondo lattice. First, we consider a single-site two-channel Kondo model. The Hamiltonian

$$H_{2\text{CK}}/J_K = \vec{S} \cdot (c_1^\dagger \vec{\sigma} c_1 + c_2^\dagger \vec{\sigma} c_2) \quad (9)$$

can be written as

$$H_{2\text{CK}}/J_K = -\frac{11}{4} + \vec{S}_{\text{tot}}^2 + \vec{C}^2 + \frac{1}{2}Q^2. \quad (10)$$

in terms of the charge and Casimirs of spin and channel

$$\vec{S}_{\text{tot}} = \vec{S} + c^\dagger \frac{\vec{\sigma}}{2} c, \quad \vec{C} = c^\dagger \frac{\vec{\tau}}{2} c, \quad Q = c^\dagger c - 2 \quad (11)$$

which are  $\vec{S}^2 = S(S+1)$  and  $\vec{C}^2 = C(C+1)$ . The energies of the 32 resulting states are listed in Table I. The ground state is the Nozières doublet corresponding to the overscreened state. This Hamiltonian can be deformed to

$$H_{2\text{CK}}^{\text{deformed}}/J_K = H_{2\text{CK}}/J_K - r_1 \vec{C}^2 - r_2 Q, \quad (12)$$

while preserving the symmetries of the Hamiltonian.  $r_1 > 2/3$  is sufficient to change the ground state to the four spin-singlet channel-doublet states. These are states

in which the impurity spin forms a spin-singlet with one of the channels. The remaining channel can be either empty or fully occupied, giving rise to the quartet. This quartet can be split by having a non-zero  $r_2$ . For example  $r_2 < 0$  will select a channel doublet with the other channel empty, and can be represented as

$$|\mu = 1/2\rangle = \frac{|\uparrow\downarrow_1 - \downarrow\uparrow_1\rangle}{\sqrt{2}}, \quad |\mu = -1/2\rangle = \frac{|\uparrow\downarrow_2 - \downarrow\uparrow_2\rangle}{\sqrt{2}}.$$

The operators  $\hat{\mathcal{O}}^\mu = \vec{S} \cdot c_a^\dagger \tau_{ab}^\mu \vec{\sigma} c_b$  act like Pauli matrices in the space of the doublet  $|\pm 1/2\rangle$ ,

$$-\frac{2}{3}\mathcal{O}^\mu \sim \tau^\mu, \quad \mu = x, y, z. \quad (13)$$

Having singled-out a channel doublet, we consider a two-channel Kondo lattice where these local ground states are coupled via the electron-hopping term. We can write

$$\begin{aligned} c_{ia\sigma} |\mu\rangle &= -\delta_{a\mu} \frac{\tilde{\sigma}}{\sqrt{2}} |\uparrow\sigma\rangle \\ c_{ia\sigma}^\dagger |\mu\rangle &= \delta_{a\mu} \frac{\tilde{\sigma}}{\sqrt{2}} |ch.T^{\tilde{a}}, \sigma\rangle \\ &\quad + \delta_{a\tilde{\mu}} [\tilde{a} \frac{\sqrt{3}}{2} |OS, \sigma\rangle + \frac{1}{2} |ch.T^0, \sigma\rangle] \end{aligned}$$

where  $\tilde{a} \equiv \text{sign}(a)$  and we have defined the Nozières over-screened excited states ( $E = -2J_K$ )

$$|OS, +1/2\rangle = \frac{1}{\sqrt{6}} |\uparrow(\uparrow_1\downarrow_2 + \downarrow_1\uparrow_2) - 2\downarrow\uparrow_1\uparrow_2\rangle \quad (14)$$

$$|OS, -1/2\rangle = \frac{1}{\sqrt{6}} |2\uparrow\downarrow_1\downarrow_2 - \downarrow(\uparrow_1\downarrow_2 + \downarrow_1\uparrow_2)\rangle \quad (15)$$

and channel triplet excited states  $|ch.\vec{T}, \sigma\rangle$ . For the sake of this section, we can project out the latter assuming that their energy is pushed further up. Therefore, the lowest excited states are the Nozières states and the empty states  $|\uparrow\sigma\rangle$ . Treating the hopping via 2nd order perturbation theory,

$$H_{\text{eff}} = -\mathcal{P} \left[ H_t \mathcal{Q} \frac{1}{\Delta H_0} \mathcal{Q} H_t \right] \mathcal{P} \quad (16)$$

where  $\mathcal{P}$  and  $\mathcal{Q}$  are projectors to ground state and excited states, respectively and  $\mathcal{P} + \mathcal{Q} = 1$ . Assuming that the sites  $i$  and  $j$  are initially at  $|\mu_i, \nu_j\rangle$  and eventually at  $|\mu'_i, \nu'_j\rangle$  we find after a straightforward calculation

$$\langle \mu'_i, \nu'_j | H_{\text{eff}} | \mu_i, \nu_j \rangle = \frac{3t^2}{4\Delta E} \mathcal{X}_{\mu\nu}^{\mu'\nu'}, \quad \mathcal{X}_{\mu\nu}^{\mu'\nu'} = -\tilde{\nu}\tilde{\nu}' \delta_{\tilde{\mu}\nu} \delta_{\tilde{\mu}'\nu'}$$

where  $\Delta E = (1 + 3r_1/2)J_K$ . It can be easily shown that  $\mathcal{X} = \mathbb{P} - \mathbb{1}$  where  $\mathbb{P}_{\mu\nu}^{\mu'\nu'} = \delta_{\mu'}^{\nu'} \delta_{\mu}^{\nu'}$  is the exchange matrix and we have the relation

$$2\mathbb{P} = \mathbb{1} + \vec{\tau}_i \cdot \vec{\tau}_j. \quad (17)$$

This completes the derivation.

					<hr/> <hr/>				
					$S$	$C$	$Q$	$\#$	$E$
$S$	$C$	$Q$	$\#$	$E$	$3/2$	$0$	$0$	$4$	$1$
$1$	$0$	$0$	$3$	$0$	$1$	$1/2$	$\pm 1$	$12$	$1/2$
$1/2$	$1/2$	$\pm 1$	$8$	$0$	$1/2$	$0$	$\pm 2$	$4$	$0$
$0$	$0$	$\pm 2$	$2$	$0$	$1/2$	$1$	$0$	$6$	$0$
$0$	$1$	$0$	$3$	$0$	$0$	$1/2$	$\pm 1$	$4$	$-3/2$
					$1/2$	$0$	$0$	$2$	$-2$

TABLE I. The spectrum of a single-site 2CK model using a  $SU_{\text{sp}}(2) \otimes SU_{\text{ch}}(2) \otimes U(1)$  symmetry labeling, (left) free electron (right) after coupling to the spin.  $S, C$  are the total spin and channel of the state and  $Q$  is the charge.

## 2. Details of numerical computation

Here we describe our algorithm to compute the low temperature Green's functions. All other physical quantities can be computed from them thanks to the large-N limit. The Green's functions are computed from the self-consistency equations,

$$\Sigma_b(j, \tau) = -\gamma G_c(j, \tau) G_\chi(j, \tau), \quad (18)$$

$$\Sigma_\chi(j, \tau) = G_c(-j, -\tau) G_b(j, \tau). \quad (19)$$

We found that they are best represented in momentum and frequency domain. The solutions are solved on linear or logarithmic frequency grids and a linear momenta grid. Using that  $G_c^{-1}(k, z) = z - \epsilon_k$ , and with  $L = \mathcal{V}$  in 1D, we find

$$\begin{aligned} \Sigma_b''(k, \omega) &= -\frac{\gamma}{L} \sum_p [f(\epsilon_p) - f(\epsilon_p - \omega)] G_\chi''(k - p, \omega - \epsilon_p), \\ \Sigma_\chi''(k, \omega) &= \frac{1}{L} \sum_p [f(\epsilon_p) + n_B(\epsilon_p + \omega)] G_b''(k + p, \omega + \epsilon_p). \end{aligned} \quad (20)$$

Thus, only a single sum over momenta is needed. Then we used Hilbert transform to recover the full self-energies. Next, the retarded Green's functions are computed from the self-energies with  $z$  set to  $\omega + i\eta$  in

$$G_b(k, z) = \frac{1}{z - \epsilon_k - \Sigma_b(k, z)}, \quad (21)$$

$$G_\chi(k, z) = \frac{1}{-1/J_K - \Sigma_\chi(k, z)}, \quad (22)$$

where  $\epsilon_k = E(k) + \mu_b$ , and  $E(k) = -2t_b \cos(k)$  was used in the main text. A binary search for  $\mu_b$  is finally used to satisfy the constraint

$$2s = -\frac{1}{L} \sum_k \int \frac{d\omega}{\pi} n_B(\omega) G_b''(k, \omega + i\eta). \quad (23)$$

The procedures above constitute the essential step in updating the self-consistency equations. Our main solver program is organized as follows:

0. Initialize the self-energies to zero at a high temperature  $T$ . Also initialize  $\mu_b$ , say, to  $T \log(1 + 1/2s)$ .
1. At present temperature  $T$ , initialize  $\eta$  to a large value, say  $T$ . Then,
  - (a) update the self-consistency equations; then
  - (b) reduce  $\eta$  and repeat Step 1a until  $\eta$  is small compare to  $T$ , say  $\eta = T/32$ ; then
  - (c) repeat 1a until Green's functions converge.
2. Reduce  $T$  and rerun Step 1. Repeat until the desired temperature is reached.

The gradual decrease of  $T$  and  $\eta$  helps with the convergence. Frequency and momenta resolution limits the convergence at low temperature. The frequency grid need to be fine enough to resolve the sharp features due to small  $T$  and  $\eta$ . For us typically  $\Delta\omega < \eta/7$ . The momenta resolution, or finite size effect, also limits the lowest temperature attainable to the order of the group velocity of conduction electrons  $v_c/L$ .

Strictly speaking,  $G_\chi(k, z)$  does not obey a Kramers-Kronig relation, whereas  $G_\chi - g_\chi$  does. Consequently,  $\Sigma_b(k, z)$  obtained above is missing a real temperature-dependent constant  $\gamma J_K \sum_p f(\epsilon_p)/L$ . This can be conveniently absorbed into  $\mu_b$  and need not be explicitly computed.

To improve efficiency, in 1D calculations inversion symmetry was assumed and only half of the momenta grid is computed without loss of generality in our study. At low temperature, the computation can be further sped up with a frequency grid that is uniform at low frequencies and logarithmic at higher ones.

### 3. Other cases

Here, we briefly present two other cases in addition to the case presented in the paper.

The first is the fully-screened case  $K = 2S$  with half-filled conduction electrons, shown in Fig. 5. This has to be contrasted to the Fermi liquid regime of the ferromagnetically coupled Kondo lattice treated in the independent bath approximation in Ref. [28]. The spectrum of spinons  $-G_b''(k, \omega + i\eta)$  and holons  $-G_\chi''(k, \omega + i\eta)$  [Fig. 5(a,b)] show that ground state is gapped. Fig. 5(c) shows that the ground state is paramagnetic, all spinons are confined to negative frequencies (as expected from spinon gap) and the electrons have a large FS, as  $v_{\chi,a}^{\text{FS}} = \pi$ . The plateau in  $v_{\chi,a}^{\text{FS}}$  is due to van Hove singularity of the conduction band density of states. Fig. 5(d) shows the conduction electron self-energy  $-N\Sigma_c''(k, \omega + i\eta)$ ,

$$-N\Sigma_{c,\text{loc}}''(\omega + i\eta) = \int \frac{dx}{\pi} [f(x) + n_B(x + \omega)] G_{\chi,\text{loc}}''(x) G_{b,\text{loc}}''(x + \omega) \quad (24)$$

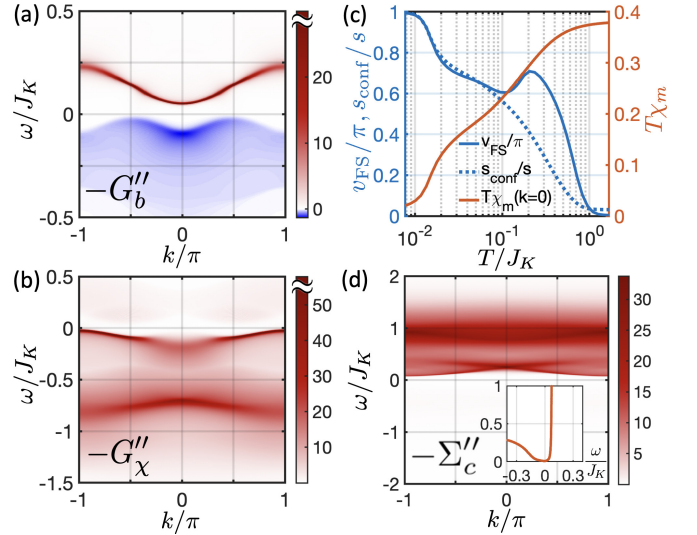


FIG. 5. Perfectly screened Kondo lattice with a finite  $t_b = 0.2t_c$  and  $J_K = 6t_c$ . The spectral weights of (a) spinons and (b) holons show dispersion on top of a gap. In (c), both the holon fermi volume,  $v_\chi^{\text{FS}}$ , and the fraction of spinons at negative frequencies,  $s_{\text{conf}}/s$ , show the onset of Kondo physics. The uniform magnetic susceptibility is also displayed as  $T\chi_m$ , showing Curie and Pauli susceptibility at high and low temperatures, respectively. (d) The imaginary part of the self-energy of conduction electrons  $-N\Sigma_c''$ . The inset shows the gap in  $-N\Sigma_{c,\text{loc}}''$  near zero frequency. Panels (a),(b) and (d) are evaluated at  $T = 0.0077J_K$ .

At zero temperature we can simplify this expression to:

$$-N\Sigma_{c,\text{loc}}''(\omega + i\eta) = \int_{-\omega}^0 \frac{dx}{\pi} G_{\chi,\text{loc}}''(x) G_{b,\text{loc}}''(x + \omega). \quad (25)$$

For the fully-screened case, spinons and holons develop a gap  $E_{\text{gap}} \sim T_K$  in their spectrum at zero temperature. Therefore, for  $|\omega| \ll E_{\text{gap}}$  this expression is equal to zero and  $-\Sigma_{c,\text{loc}}''$  is also gapped. This is in agreement with the numerical results shown in Fig. 5(d).

The second case is a four-channel Kondo case  $K = 8S$  with a band of 3/4-filled conduction electrons in Fig. 6. For an infinitesimal  $t_b$  the low energy spectrum shows unit cell-doubling and consequently two pairs of low-energy spinon and holon modes. A stronger  $t_b$  breaks the symmetry between these two pairs.

### 4. Emergent dispersion

According to the self-consistency equations in Eqs. (18)–(22), if the input  $G_b$  and  $G_\chi$  are both local and  $t_b = 0$ , then the updated Green's functions will remain local. Thus naively, without  $t_b$  any Kondo lattice problem always reduces to a 0D impurity one. As shown in the main text, the 1D 2CKL is quite different from the impurity case when  $t_b \neq 0$ . Decreasing  $t_b$  from large values will decrease the bandwidths of low energy spinon



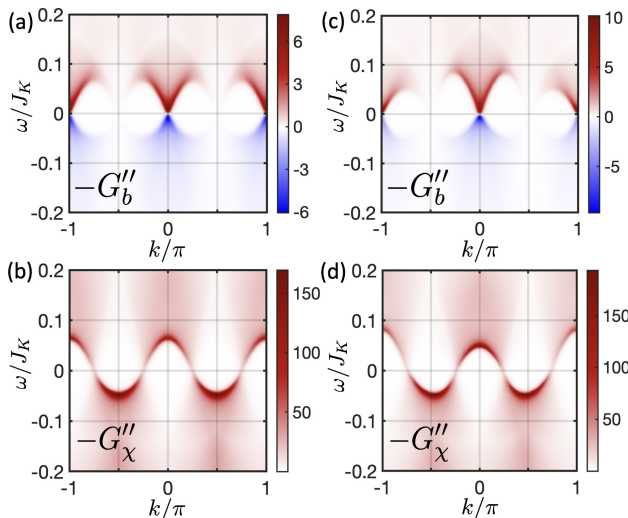


FIG. 6. Double-screened Kondo lattice ( $K/2S = 2$ ) with 3/4-filled conduction electrons and spinon hoppings that are: (a–b) infinitesimal,  $t_c/t_b = 0.002t_c$ , and (c–d) finite,  $t_b = 0.2t_c$ . The spectral weights of spinons and holons show emergent Lorentz invariant modes similar to the half-filled case, but a doubled unit cell under infinitesimal  $t_b$ . The case of finite  $t_b$  breaks the symmetry between modes around  $k = 0$  and  $\pi$ . Here  $J_K = 6t_c$ , and  $T = 0.004J_K$  in both cases.

and holon modes, but below a certain  $t_b^*$ , these bandwidths will remain the same. This is the emergent dispersion dynamically generated due to an amplification of RKKY, as illustrated in Fig. 2.

The emergent dispersion lowers the free energy of the system compared to the local solution, as seen in the entropy inset of Fig. 2(b). At high temperature, denoted by  $T_h$ , the 0D and infinitesimal- $t_b$  1D state have the same entropy  $S$  and free energy  $F$ . At low temperature, denoted by  $T_l$ ,  $S_{0D} > S_{1D}$ . Since  $F(T_l) = F(T_h) - \int_{T_l}^{T_h} SdT$ , the solution of 1D' gives a lower free energy. Therefore it is the genuine solution of the system.

This phenomenon is best demonstrated in a seeding numerical experiment for the zero static hopping case, i.e.,  $t_b = 0$ . Here, before the self-consistency loop starts at each  $T$ , we add a tiny  $k$ -dependent  $\tilde{\Sigma}(k, \omega)T$  to the self-energy of spinons (or holons) used to construct the Green's function, which is at Step 1 of the solver. The form of this seed ensures that it scales down at lower  $T$ , and the  $\omega$  dependence is nonessential. At high temperature,  $\tilde{\Sigma}$  is rapidly suppressed by the self-consistency iterations and the Green's functions remain local, as seen in Fig. 7(a,b). Below a certain temperature, a part of the dispersion is exponentially amplified until it saturates.

Another way to observe this effect is to use an infinitesimal  $t_b \ll t_b^*$ . The emergent dispersion will then dominate the shape of low energy modes. This is also manifested in  $J_{\text{eff}}^{-1}$  and  $\varepsilon_{\text{eff}}$ , as shown in Fig. 2. In comparison to the case with a finite  $t_b = 0.2t_c$  in Fig. 7(c), we see that their behaviors are qualitatively the same.

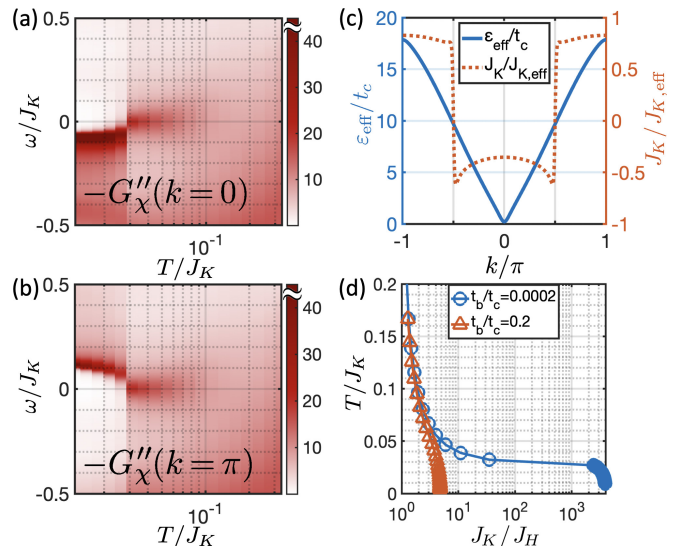


FIG. 7. (a–b) Without  $J_H$ , holon (and spinon) dispersion can emerge below some temperature in the presence of a tiny seed at the beginning of the self-consistency loop at each  $T$ . (c) The effective spinon energy and Kondo coupling for 1D 2CKL at  $t_b = 0.2t_c$ . The low temperature behavior here (at  $T = 0.0044J_K$ ) is similar to the case with an infinitesimal  $t_b$  in Fig. 2. (d) Effective Heisenberg coupling in 1D 2CKL for an infinitesimal and finite  $t_b$ .

Therefore, both the infinitesimal and finite  $t_b$  case we discussed flow to the same fixed point.

Without  $t_b$ , the Lagrangian of Eq. (2) is invariant under simultaneous Galilean boosts of spinons and holons, that is  $(b_j, \chi_j) \rightarrow e^{ikj}(b_j, \chi_j)$ . Consequently, the emergent dispersing mode here can freely translate in  $k$ . In the numerics, the exact form of  $\tilde{\Sigma}$  will determine the center of this dispersion. Different forms of  $\tilde{\Sigma}$ , including longer range hoppings, e.g.,  $\cos(nk)$ , and random self-energy seeds all yield the same low energy spectrum up to momentum translations. Therefore, it is a robust feature of the 1D Kondo lattice. Without loss of generality, we set the center of emergent spinon dispersions to  $k = 0$ .

Another manifestation of the emergent dispersion is the behavior of effective  $J_H$  as the system cools down. In 1D, variational principle applied to  $t_b$  gives [28, 37]

$$J_H^{-1} = \frac{1}{L} \frac{1}{2t_b} \sum_j \langle b_j^\dagger b_{j+1} + \text{h.c.} \rangle \quad (26)$$

$$= -\frac{1}{L} \sum_k \int \frac{d\omega}{\pi t_b} n_B(\omega) \cos(k) G_b''(k, \omega + i\eta). \quad (27)$$

For a fixed  $t_b > t_b^*$ , Fig. 7(c) shows that  $J_H$  gradually decreases with  $T$  until it settles at a finite zero-temperature value. For  $t_b \ll t_b^*$ , we see that when the dispersion emerges, the effective  $J_H$  has a steep drop to a value close to zero. This shows that no Heisenberg coupling is needed in 1D for the spinons to become mobile.



## 5. Susceptibilities

### Channel Susceptibility

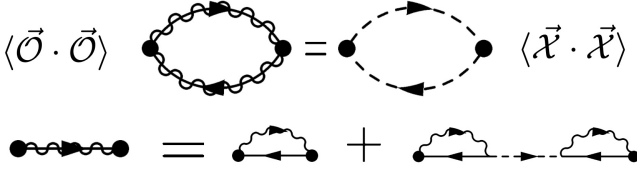


FIG. 8. Equivalence of  $\langle \vec{O} \cdot \vec{O} \rangle$  and  $\langle \vec{\mathcal{X}} \cdot \vec{\mathcal{X}} \rangle$ .

In presence of channel anisotropy,

$$H = H_c + \sum_j c_{j,\alpha\alpha}^\dagger \left( J_K \delta_{ab} + \Delta \vec{J}_j \cdot \vec{\tau}_{ab} \right) c_{j,b\beta} S_{j,\beta\alpha}, \quad (28)$$

the holon term in the Lagrangian is modified to

$$\frac{1}{J_K} \sum_j \bar{\chi}_{j,a} \chi_{j,a} \rightarrow \frac{1}{J_K} \sum_j \bar{\chi}_{j,a} \left[ \left( \mathbb{1} + \frac{\Delta \vec{J}_j \cdot \vec{\tau}}{J_K} \right)^{-1} \right]_{ab} \chi_{j,b}$$

Here  $\tau^i$  with  $i = 1 \dots K^2 - 1$  are generators of  $\text{SU}(K)$  normalized according to  $\text{Tr}[\tau^i \tau^j] = \frac{1}{2} \delta^{ij}$ . Expanding in small  $\Delta J$ , the Lagrangian is changed by

$$\begin{aligned} \Delta \mathcal{L}[\Delta J] = & - \sum_j \bar{\chi}_{j,a} \frac{\Delta \vec{J}_j \cdot \vec{\tau}_{ab}}{J_K^2} \chi_{j,b} \\ & + \sum_{j,ik} \bar{\chi}_{j,a} \frac{\Delta J_{j,i} \Delta J_{j,k} (\tau^i \tau^k)_{ab}}{J_K^3} \chi_{j,b}, \quad (29) \end{aligned}$$

up to  $O(\Delta J^2)$ . The channel susceptibility can be derived from taking derivatives of  $\log Z$  w.r.t.  $\Delta J$ . We define

$$\chi_{\text{ch}}(\vec{r}) \equiv \sum_i \left. \frac{\partial^2 \ln Z + \partial^2 \ln \det[\beta(J_K + \Delta J^{ab})]}{\partial(\Delta J_{\vec{r}}^i) \partial(\Delta J_0^i)} \right|_{\Delta J=0} \quad (30)$$

where  $\vec{r} \equiv (j, \tau)$ . Here the second term  $-\ln \det[\beta(J_K + \Delta J)]$  comes from the free path integral of the Hubbard-Stratonovitch field  $\chi$  which must be subtracted from the free energy. The first term gives

$$\begin{aligned} \left. \frac{\partial^2 \ln Z}{\partial(\Delta J_{\vec{r}}^i) \partial(\Delta J_0^i)} \right|_{\Delta J=0} = & \frac{1}{J_K^4} [\tau_{ab}^i \tau_{cd}^i \langle (\bar{\chi}_a \chi_b)_{\vec{r}} (\bar{\chi}_c \chi_d)_{\vec{0}} \rangle_{\text{lc}} \\ & - 2J_K \tau_{ac}^i \tau_{cb}^i \langle \bar{\chi}_a \chi_b \rangle \delta(\vec{r})], \quad (31) \end{aligned}$$

where  $\langle A(\vec{r}) B(\vec{t}) \rangle_{\text{lc}} \equiv \langle A(\vec{r}) B(\vec{t}) \rangle - \langle A(\vec{r}) \rangle \langle B(\vec{t}) \rangle$  denoting the linked clusters. In the large- $N$  limit,  $\langle \chi_a \bar{\chi}_b \rangle = -G_\chi \delta_{ab}$ . Noting that  $g_\chi(\vec{r}) = -J_K \delta(\vec{r})$ , R.H.S. becomes

$$J_K^{-4} [G_\chi(\vec{r}) G_\chi(-\vec{r}) + 2G_\chi(\vec{r}) g_\chi(\vec{r})] \text{Tr} [\tau^i \tau^i]. \quad (32)$$

The second term in Eq. (30) gives the same expression as Eq. (32) with an opposite sign and all  $G_\chi \rightarrow g_\chi$ . Therefore, we find for the channel susceptibility with

$$\chi_{\text{ch}}(\vec{r}) = J_K^{-4} [G_\chi(\vec{r}) - g_\chi(\vec{r})] [G_\chi(-\vec{r}) - g_\chi(-\vec{r})]. \quad (33)$$

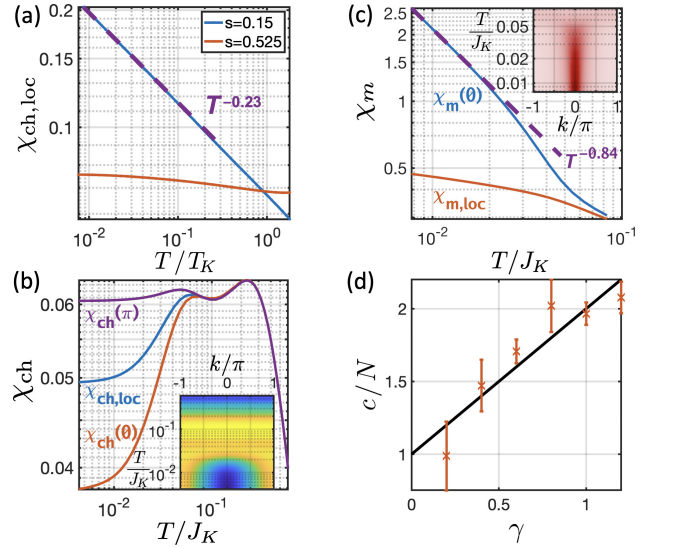


FIG. 9. (a) Local static channel susceptibility of a double-screened 0D Kondo impurity, or a 1D chain without  $J_H$ . A diverging case at  $s = 0.15$ , and a vanishing case at  $s = 0.525$  are shown. Power laws can only be extracted from diverging cases. (b) Static channel susceptibilities,  $\chi_{\text{ch,loc}}$  and  $\chi_{\text{ch}}(q)$ , of an 1D 2CKL with  $s = 0.15$ . They are vanishing as  $T \rightarrow 0$  for all  $s$ . Inset shows the momenta resolved static  $\chi_{\text{ch}}(q)$ . The 1D case here has  $J_K = 6t_c$  and  $t_b = 0.2t_c$ . (c) Uniform  $[\chi_m(q=0)]$  and local ( $\chi_{m,loc}$ ) static magnetic susceptibility of 1D 2CKL with  $s = 0.3$  and  $\Delta_b = 0.29$ . Inset shows evolution of  $\chi_m(q, \omega = 0)$  with  $T$ . (d) The central charge  $c$  extracted from heat capacity  $C/T = (\pi k_B^2/6v)c$ .

This expresses  $\chi_{\text{ch}}$  using  $\langle \mathcal{X} \mathcal{X} \rangle$  correlators.

On the other hand, from the  $\langle \vec{O} \cdot \vec{O} \rangle$  Feynman diagrams in Fig. 8 we have

$$\langle \vec{O}(\vec{r}) \cdot \vec{O} \rangle = \delta G_\chi(\vec{r}) \delta G_\chi(-\vec{r}), \quad (34)$$

where  $\delta G_\chi$  is defined as

$$\delta G_\chi(\vec{r}) \equiv \Sigma_\chi(\vec{r}) + \sum_{\vec{r}_1 \vec{r}_2} \Sigma_\chi(\vec{r} - \vec{r}_1) G_\chi(\vec{r}_1 - \vec{r}_2) \Sigma_\chi(\vec{r}_2) \quad (35)$$

In momentum and frequency space

$$\delta G_\chi(k, z) = \Sigma_\chi(1 + G_\chi \Sigma_\chi) = \frac{1}{J_K^2} [G_\chi(k, z) + J_K] \quad (36)$$

Thus,  $\delta G_\chi = (G_\chi - g_\chi)/J_K^2$ . Therefore, as Fig. 8 suggests, the two approaches agree.

In Fig. 9(a,b), we show the static channel susceptibilities of the 0D and 1D 2CKL. As discussed in the main text, in all dimensions the local susceptibility is  $\chi_{\text{ch}}(x=0) = \int_0^\beta d\tau \delta G_\chi(0, \tau) \delta G_\chi(0, -\tau) \sim T^{4\Delta_x - 1}$ , and in 1D the uniform susceptibility is  $\chi_{\text{ch}}^{\text{1D}}(q=0) = \int d^2 r \delta G_\chi(\vec{r}) \delta G_\chi(-\vec{r}) \sim T^{4\Delta_x - 2}$ . For 0D or  $\infty$ D, the  $\chi_{\text{ch}}(x=0)$  changes from diverging to vanishing at low temperature as  $s$  increases, according to Eq. (5). For 1D, the static channel susceptibilities are always vanishing

according to Eq. (8). Since the Green's functions we computed have both a scaling part and a regular part, only diverging scaling laws may be reliably extracted. The regular part will typically overwhelm the vanishing components, except at very low (zero) frequencies as is the case for  $v_\chi^{\text{FS}}$  [Fig. 4(a)].

### Magnetic susceptibility

We show the magnetic susceptibilities in 1D for  $s = 0.3$  in Fig. 9(c). Here the uniform static magnetic susceptibility  $\chi_m(q = 0)$  is diverging, revealing a magnetic instability as discussed in the main text. The local static susceptibility  $\chi_m(x = 0)$  is vanishing in this case, but diverges for  $s > 0.375$ . The inset shows  $\chi_m(q)$  vs.  $T$ . At low  $T$ ,  $\chi_m(q)$  becomes sharply peaked at  $q = 0$ .

## 6. Scaling analysis for impurity problem

For the sake of completeness, we review the scaling analysis for the multi-channel Kondo problem using Schwinger bosons [37], which also applies to the infinite-coordination lattice problem we have studied in this paper. For the spinon and holon we use the  $T = 0$  ansatz

$$G_b(\tau) = b_b \frac{1}{|\tau|^{2\Delta_b}}, \quad G_\chi(\tau) = b_\chi \frac{\text{sign}\tau}{|\tau|^{2\Delta_\chi}}. \quad (37)$$

Using the self-energy formulae

$$\Sigma_B(\tau) = -\gamma g_c(\tau) G_\chi(\tau), \quad \Sigma_\chi(\tau) = g_c(-\tau) G_B(\tau), \quad (38)$$

and that the Green's function is  $g_c(\tau) = -\rho_c/\tau$  we have

$$\Sigma_b(\tau) = -b_\chi \gamma \rho_c \frac{\text{sign}\tau}{|\tau|^{2\Delta_\chi+1}}, \quad \Sigma_\chi(\tau) = b_b \rho_c \frac{\text{sign}\tau}{|\tau|^{2\Delta_b+1}},$$

Fourier transform of the Green's function are

$$G_b(i\omega) = 2b_b |\omega|^{2\Delta_b-1} \Gamma(1-2\Delta_b) \sin \pi \Delta_b$$

$$G_\chi(i\omega) = 2b_\chi |\omega|^{2\Delta_\chi-1} \Gamma(1-2\Delta_\chi) \cos \pi \Delta_\chi \text{sign}(\omega)$$

with similar expressions for  $\Sigma_b$  and  $\Sigma_\chi$ .  $G_c$  can be computed from  $G_\chi$  in the  $\Delta_\chi \rightarrow 1/2$  limit. The zero and the pole of  $G_c$  cancel each other in this limit. Next we plug these into the Dyson equations:

$$G_b(i\omega)[i\omega - \lambda - \Sigma_b(i\omega)] = 1, \quad G_\chi(i\omega)[-J_K^{-1} - \Sigma_\chi(i\omega)] = 1.$$

In the scaling limit, the numerical solutions show that  $G_\chi \Sigma_\chi = G_b \Sigma_b = -1$ . For this equation to hold, the powers of frequency have to cancel from the left side, i.e.  $2\Delta_b + 2\Delta_\chi = 1$ , and the amplitudes must match, i.e.

$$4\gamma b_b b_\chi \sin^2 \pi \Delta_b \Gamma(1-2\Delta_b) \Gamma(2\Delta_b-1) = -1,$$

$$4\rho b_\chi b_b \sin^2 \pi \Delta_b \Gamma(2\Delta_b) \Gamma(-2\Delta_b) = -1. \quad (39)$$

Using  $\Gamma(z+1) = z\Gamma(z)$ , the ratio finally gives

$$2\Delta_b = \frac{1}{1+\gamma}, \quad 2\Delta_\chi = \frac{\gamma}{\gamma+1}. \quad (40)$$

For the case of  $\infty D$  Bethe lattice, we can write

$$G_b^{-1} = \Omega_x - t_x^2 G_x, \quad (41)$$

for  $x = b, c$  where  $\Omega_c(z) = z - \mu_c$  but  $\Omega_b(z) = z - \mu_b - \Sigma_b(z)$ . The solution is

$$t_x G_x = \Omega_x / 2t_x - \text{sign}(\Omega'_x) \sqrt{(\Omega_x / 2t_x)^2 - 1}. \quad (42)$$

We are interested in the  $t_b \rightarrow 0$  limit of this expression. We find not surprisingly that

$$t_b G_b = (\Omega_b / 2t_b) [1 - \sqrt{1 + (2t_b / \Omega_b)^2}] \approx t_b / \Omega_x, \quad (43)$$

showing that in this limit the lattice is dominated by the local impurity solution and so, exponents are the same.

## 7. Details of scaling analysis in 1D case

This section follows closely the impurity solution. We use the symbol  $\sqrt{a} b_j(\tau) \sim b(x, \tau)$  for  $x = ja$  to refer to the low-momentum  $k \sim 0$  content of the spinons. We also expand fermionic field around the Fermi energy:

$$\sqrt{a} c_j(\tau) \sim e^{ik_F x} c_R(x, \tau) + e^{-ik_F x} c_L(x, \tau) \quad (44)$$

$$a^\xi \chi_j(\tau) \sim e^{ik_F x} \chi_R(x, \tau) + e^{-ik_F x} \chi_L(x, \tau) \quad (45)$$

The interaction term becomes

$$H_{\text{int}} = a^\xi \sum_{\alpha\alpha} \int dx [(\chi_{R\alpha}^\dagger c_{L\alpha}^\dagger + \chi_{L\alpha}^\dagger c_{R\alpha}^\dagger) b_\alpha + h.c.]. \quad (46)$$

This leads to the self-energies

$$\Sigma_{\chi R/L}(\vec{r}) = G_{cL/R}(-\vec{r}) G_b(\vec{r}) \quad (47)$$

$$\Sigma_b(\vec{r}) = -\gamma [G_{cR}(\vec{r}) G_{\chi L}(\vec{r}) + G_{cL}(\vec{r}) G_{\chi R}(\vec{r})]$$

In terms of these, the lattice Green's functions are

$$a \check{g}_c(x, \tau) = e^{ik_F x} g_R(x, \tau) + e^{-ik_F x} g_L(x, \tau), \quad (48)$$

$$a^{2\xi} \check{G}_\chi(x, \tau) = e^{ik_F x} G_{\chi R}(x, \tau) + e^{-ik_F x} G_{\chi L}(x, \tau), \quad (49)$$

$$a \check{G}_b(x, \tau) = G_b(x, \tau). \quad (50)$$

The ansatzes put forward in the paper are

$$G_b = -\bar{\rho} \left( \frac{a^2}{\bar{z}z} \right)^{\Delta_b}, \quad G_{\chi R/L} = \frac{-1}{2\pi} \left( \frac{a}{\bar{z}} \right)^{\Delta_\chi \pm \frac{1}{2}} \left( \frac{a}{z} \right)^{\Delta_\chi \mp \frac{1}{2}}.$$

The Fourier transform of the imaginary-time function is straightforward:

$$G_b(k, i\omega) = -\bar{\rho} \int_{-\infty}^{+\infty} dx \int_{-\infty}^{+\infty} d\tau e^{-i(kx - \omega\tau)} \left( \frac{a^2}{\bar{z}z} \right)^{\Delta_b} \quad (51)$$

Defining  $z \equiv u\tau + ix = re^{i\phi}$  and  $q \equiv k + i\omega/u = |q|e^{i\theta}$ ,

$$kx - \omega\tau = \text{Im}[z\bar{q}] = r|q|\sin(\phi - \theta), \quad (52)$$

and we have

$$G_b(k, i\omega) = -2\pi\bar{\rho}u_b^{-1} \int r dr \int_0^{2\pi} \frac{d\phi}{2\pi} e^{-i|q|r\sin(\phi-\theta)} \left(\frac{a^2}{r^2}\right)^{\Delta_b}$$

This integral is the  $n = 0$  version of a more general integral that we will encounter again. So, let us define

$$\begin{aligned} \mathcal{I}_{n,\Delta}(q) &\equiv \int r dr \left(\frac{a^2}{r^2}\right)^\Delta \int \frac{d\phi}{2\pi} e^{-i[r|q|\sin(\phi-\theta)+n\phi]} \\ &= a^2 |qa|^{2(\Delta-1)} (-1)^n e^{-in\theta} \zeta_n(\Delta), \end{aligned} \quad (53)$$

where we have used a  $\phi \rightarrow \phi + \theta - \pi/2$  shift to write it in terms of the  $\zeta$  function

$$\zeta_n(\Delta) \equiv \int_0^\infty dx x^{1-2\Delta} R_n(x), \quad (54)$$

which by itself is written in terms of

$$\begin{aligned} R_n(x) &\equiv (-i)^n \int_0^{2\pi} \frac{d\phi}{2\pi} e^{-in\phi} e^{ix \cos \phi} \\ &= (-i)^n \int_0^{2\pi} \frac{d\phi}{2\pi} e^{-in\phi} \sum_m i^m J_m(x) e^{im\phi} = J_n(x). \end{aligned}$$

Therefore, the zeta-function is nothing but the *Melin transform* of the Bessel function:

$$\zeta_{n \geq 0}(\Delta) = 2^{1-2\Delta} \frac{\Gamma(1 - \Delta + n/2)}{\Gamma(\Delta + n/2)}, \quad (55)$$

valid for  $\Delta > 1/4$  and  $n > -3/2$  and  $\Delta < 1 + n/2$ . Since  $J_{-n}(x) = (-1)^n J_n(x)$  we can express  $\zeta_{-n}(\Delta) = (-1)^n \zeta_{n > 0}(\Delta)$  in terms of  $\zeta_{n \geq 0}$ . Using the  $\mathcal{I}_{0,\Delta}(q)$  integral we readily find

$$G_b(k, i\omega) = -2\pi\bar{\rho}a^2 u_b^{-1} |aq|^{2(\Delta_b-1)} \zeta_0(\Delta_b), \quad (56)$$

where  $\zeta_0(\Delta) = 2^{1-2\Delta} \Gamma(1 - \Delta) / \Gamma(\Delta)$  from Eq. (55). Analytical continuation  $i\omega \rightarrow \omega + i\eta$  leads to

$$\begin{aligned} G_b''(k, \omega + i\eta) &= (\bar{\rho}a) a u_b^{-1} \left| \frac{\omega^2 - u^2 k^2}{4u a^{-2}} \right|^{\Delta-1} \Gamma^2(1 - \Delta) \\ &\times \frac{1}{2} \sin^2 \pi \Delta \sin \left[ \text{sign}(\omega/u + k) + \text{sign}(\omega/u - k) \right]. \end{aligned} \quad (57)$$

For the holons we have

$$\begin{aligned} G_{\chi R}(k, i\omega) &= -\frac{u_\chi^{-1}}{2\pi} \int_{-\infty}^{+\infty} dx \\ &\int_{-\infty}^{+\infty} d\tau e^{-i(kx - \omega\tau)} \left(\frac{a^2}{x^2 + u^2 \tau^2}\right)^\Delta e^{+i\angle(u\tau + ix)} \end{aligned} \quad (58)$$

This is the  $n = -1$  case of  $\mathcal{I}_{n,\Delta}(q)$  integral. Therefore,

$$G_{\chi R}(k, i\omega) = -u_\chi^{-1} a^{2(1-\xi)} (\bar{q}qa^2)^{(\Delta-1)} \frac{|q|}{q} \zeta_1(\Delta), \quad (59)$$

and similarly for left-movers

$$G_{\chi L}(k, i\omega) = u_\chi^{-1} a^{2(1-\xi)} (\bar{q}qa^2)^{(\Delta-1)} \frac{|q|}{q} \zeta_1(\Delta). \quad (60)$$

We use these to find the Fourier transform of lattice Green's functions. Defining shifted variables

$$q_n \equiv (k - nk_F) + i\omega/u, \quad \theta_n \equiv \angle[(k - nk_F) + i\omega/u]$$

and using  $\zeta_1(1/2) = 1$ , the lattice Green's functions are

$$a\check{G}_b(k, i\omega) = -2\pi \frac{\bar{\rho}a^2}{u_b} \zeta_0(\Delta_b) |aq|^{2\Delta_b-2} \quad (61)$$

$$a\check{g}(k, i\omega) = \frac{a}{v_F} \left[ \frac{-1}{\bar{q}_1} \right] + \frac{a}{v_F} \left[ \frac{1}{q_{-1}} \right] \quad (62)$$

$$\begin{aligned} a^{2\xi} \check{G}_\chi(k, i\omega) &= \frac{a^2}{u_\chi} \zeta_1(\Delta_\chi) \left\{ -|aq_1|^{2(\Delta_\chi-2)} \frac{|q_1|}{\bar{q}_1} \right. \\ &\quad \left. + |aq_{-1}|^{2(\Delta_\chi-2)} \frac{|q_{-1}|}{q_{-1}} \right\}. \end{aligned} \quad (63)$$

Assuming that the bare Green's functions computed above are the exact ones the self-energy of bosons is

$$a^{1+2\xi} \Sigma_b(x, \tau) = -\frac{\gamma}{2\pi^2} \left(\frac{a^2}{\bar{z}z}\right)^{\Delta_\chi+1/2} \quad (64)$$

and the self-energies of the holon is

$$a^2 \Sigma_{\chi R/L}(x, \tau) = -\frac{\bar{\rho}}{2\pi} \left(\frac{a^2}{\bar{z}z}\right)^{\Delta_b+1/2} e^{\pm i\angle z} \quad (65)$$

To have conformal invariance, we have assumed all the velocities are the same  $u_b = u_\chi = u_c = u$  and holons and conduction electrons have the same Fermi wavevectors. The Fourier transform can be computed as before:

$$a^{1+2\xi} \Sigma_b(k, i\omega) = -\gamma \frac{a^2}{\pi u} \zeta_0(\Delta_\chi + 1/2) |aq|^{2\Delta_\chi-1} \quad (66)$$

$$a^2 \Sigma_{\chi R/L}(k, i\omega) = \mp \frac{\bar{\rho}a^2}{u} \zeta_1(\Delta_b + 1/2) e^{\pm i\theta} \quad (67)$$

For the self-consistency, we have to note that  $G\Sigma \propto a^{1-2\xi}$  and we must choose  $\xi = 1/2$ . To first approximation, we neglect the  $2k_F$  contributions. The self-consistency, then leads to [Note that in the second line, the signs do not match for  $\Delta_\chi \in (0, 0.5)$ , therefore  $\Delta_\chi \notin (0, 0.5)$ .]

$$G_b \Delta \Sigma_b = -1 \quad \rightarrow \quad 2\gamma A \left[ \zeta_0(\Delta_b) \zeta_0(\Delta_\chi + 1/2) \right] = -1$$

$$G_{\chi R/L} \Delta \Sigma_{\chi R/L} = -1 \quad \rightarrow \quad A \left[ \zeta_1(\Delta_b + 1/2) \zeta_1(\Delta_\chi) \right] = 1$$

where we defined  $A = \bar{\rho}a/u_\chi u_b$ . Eliminating  $A$  between these equations, and using  $\Delta_b = 3/2 - \Delta_\chi$  we find

$$2\gamma = -\frac{\zeta_1(2 - \Delta_\chi) \zeta_1(\Delta_\chi)}{\zeta_0(3/2 - \Delta_\chi) \zeta_0(\Delta_\chi + 1/2)} \quad (68)$$

To solve this equation, we use the relation  $\Gamma(\Delta)\Gamma(1 - \Delta) = \pi/\sin \pi\Delta$ , the  $\zeta$  function can be written as

$$\zeta_n(\Delta) = 2^{1-2\Delta} \frac{\sin \pi(n/2 + \Delta)}{\pi} \Gamma(1 - \Delta + n/2) \Gamma(1 - \Delta - n/2)$$

This equation, together with  $\Delta_1 + \Delta_2 = 2$  and  $\sin(\pi z)\Gamma(z)\Gamma(-z) = -\pi/z$  can be used to prove that

$$\zeta_n(\Delta_1)\zeta_n(\Delta_2) = \frac{-1/4}{(1 - \Delta_1)^2 - n^2/4},$$

for  $n = 0, 1$ . Using these we find the solution

$$2\gamma = -\frac{(\Delta_\chi - 1/2)^2}{(\Delta_\chi - 1)^2 - 1/4} \quad (69)$$

which leads to

$$\Delta_\chi = \frac{1 + 6\gamma}{2(1 + 2\gamma)}, \quad \Delta_b = \frac{3}{2} - \Delta_\chi = \frac{2}{2(1 + 2\gamma)}. \quad (70)$$

### 8. A Luttinger liquid model

The form of the Green's functions are fixed due to conformal invariance. The simplest theory that can lead to such correlation functions is three Luttinger liquids:

$$H_0 = a^\xi \sum_{\zeta=c,b,\chi} \frac{u_\zeta}{2\pi} \int dx [K_\zeta (\partial_x \phi^\zeta)^2 + K_\zeta^{-1} (\partial_x \theta^\zeta)^2], \quad (71)$$

where the new bosons  $\phi$  and  $\theta$  obey

$$[\phi^\zeta(x), \theta^{\zeta'}(y)] = -\frac{i\pi}{2} \text{sign}(x - y) \delta^{\zeta\zeta'} \quad (72)$$

While we haven't written the spin and channel indices explicitly, it is clear that  $\phi^c = \phi_{a\alpha}^c(x)$  and  $\phi^\chi = \phi_a^\chi(x)$  and so on. In terms of these bosons, the holon fields are

$$\chi_R = \frac{a^{-1/2}}{\sqrt{2\pi}} e^{i(\phi^\chi - \theta^\chi)}, \quad \chi_L = \frac{a^{-1/2}}{\sqrt{2\pi}} e^{i(\phi^\chi + \theta^\chi)} \quad (73)$$

(similar expression for electrons) whereas the spinons are

$$b = \sqrt{\rho} e^{i\phi^b}, \quad \rho = \bar{\rho} - \frac{1}{\pi} \partial_x \theta^b \quad (74)$$

and the Luttinger parameters  $K_\zeta$  are fixed to produce the correct exponents. For conduction electrons  $K_c = 1$  so  $\Delta_c = 1/2$ . But for the spinon and holon we must have

$$4\Delta_b = K_b^{-1}, \quad 4\Delta_\chi = K_\chi + K_\chi^{-1} \quad (75)$$

Note that the interaction  $H_{\text{int}}$  in Eq.(46) is truly marginal at the IR fixed point we have found. In the bosonized language, the interaction becomes

$$H_{\text{int}} = 4a^\xi \sum_{\alpha\alpha'} \int dx \cos(\phi_\alpha - \phi_a - \phi_{a\alpha}) \cos(\theta_a - \theta_{a\alpha})$$

while we have omitted the boson flavors, it's obvious that  $\phi_\alpha = \phi_\alpha^b$  and  $\phi_a = \phi_a^\chi$  and so on. The interacting Luttinger liquid  $H = H_0 + H_{\text{int}}$  describes a conformally invariant fixed point. Our Luttinger liquid model predicts that the central charge of the spinons and holons is  $c_0 = (1 + \gamma)N$ . This is confirmed by the heat capacity extracted from the numerics as  $T \rightarrow 0$ , as plotted in Fig. 9(d). The error mainly comes from fitting the group velocity of the low energy modes. Within error, the numerics agree with the Luttinger liquid model. We conjecture that  $a^\xi$  with  $\xi = 1/2$  prefactor in Eq. (71) makes it irrelevant  $H_{\text{int}} \rightarrow 0$  in the continuum limit.

### 9. Large-N limit of the Andrei-Orignac Coset theory

According to [25], using non-abelian bosonization in the limit of large Heisenberg coupling between spins and away from any charge commensurate filling, the Hamiltonian can be written in the form of  $\vec{J}_L \cdot \vec{S}_R + \vec{J}_R \cdot \vec{S}_L$  where  $\vec{S}_{R/L}$  are  $SU_1(2)$  right/left-mover currents describing local moments and  $\vec{J}_{R/L}$  are  $SU_K(2)$  right/left-mover currents describing the spin sector of fermions. Ref. [25] shows that this system flows to the so-called chirally-stabilized fixed point, described by the coset theory,

$$c_{AO}(2, K) \equiv c \left[ \frac{SU_K(2) \times SU_1(2)}{SU_{K+1}(2)} \right] \quad (76)$$

$$= 1 - \frac{6}{(K+1)(K+2)} = 0, \frac{1}{2}, \frac{7}{10}, \frac{4}{5}, \dots$$

For  $K = 2$  a dispersing Majorana model is predicted. Assuming that  $\vec{J}_{R/L}$  and  $\vec{S}_{R/L}$  are currents of  $SU(N)$  WZW models, we propose a generalization of this theory

$$c_{AO}(N, K) \equiv c \left[ \frac{SU_K(N) \otimes SU_1(N)}{SU_{K+1}(N)} \right] \quad (77)$$

$$= (N^2 - 1) \left[ \frac{K}{N+K} + \frac{1}{N+1} - \frac{K+1}{N+K+1} \right].$$

In the limit of large-N we find

$$\lim_{N \rightarrow \infty} \frac{1}{N} c_{AO}(N, \gamma N) = 1 - \frac{1}{(1 + \gamma)^2}. \quad (78)$$